Aggregate

WILEY

Aggregate

RESEARCH ARTICLE OPEN ACCESS

Pathway Complexity in Supramolecular Polymerization of Porphyrin Dyads for Kinetic Control of Helicity

Hosoowi Lee[1] | Yongho Lee[2] | Minhyeong Lee[2] | Dae Eun Kang[2] | Jiwon Kim[1] | Dong Ha Kim[1] | Woo-Dong Jang[2]

[1]Department of Chemistry and Nanoscience, Ewha Womans University, Seodaemun-gu, Seoul, Republic of Korea | [2]Department of Chemistry, Yonsei University, Seodaemun-gu, Seoul, Republic of Korea

Correspondence: Woo-Dong Jang (wdjang@yonsei.ac.kr)

Received: 22 April 2025 | **Revised:** 1 June 2025 | **Accepted:** 9 June 2025

Funding: This work was supported by the National Research Foundation (NRF) grant (RS-2025-00514482, RS-2024-00345550) funded by the Ministry of Science and ICT (MSIT), Korea.

Keywords: circular dichroism | circularly polarized luminescence | pathway complexity | porphyrins | supramolecular polymers

ABSTRACT

The supramolecular polymerization of porphyrin dyad (**PD**) shows the pathway complexity leading to the formation of kinetically metastable nanoparticles ($\mathbf{PD}_{\mathbf{Particle}}$) through rapid cooling and thermodynamically stable fibrous supramolecular polymers ($\mathbf{PD}_{\mathbf{Fiber}}$) through slow cooling. The kinetically metastable $\mathbf{PD}_{\mathbf{Particle}}$ is gradually transformed to the thermodynamically stable $\mathbf{PD}_{\mathbf{Fiber}}$. Due to the inherent achirality of **PD**, AFM images exhibited a random distribution of both *M* and *P* helices. Introducing chiral alkyl chains achieved a predominant helicity in $\mathbf{PD}_{\mathbf{Fiber}}$, with (*S*)-**PD** favoring *M* helices and (*R*)-**PD** favoring *P* helices. The addition of chiral 2-methyl pyrrolidine (MePy) further influences this transformation by retarding the transition from $\mathbf{PD}_{\mathbf{Particle}}$ to $\mathbf{PD}_{\mathbf{Fiber}}$ through axial coordination with the zinc porphyrin units, affecting the helicity of the resulting supramolecular polymer. By manipulating the cooling rates and environmental conditions, we demonstrate the reversible control over circular dichroism (CD) and circularly polarized luminescence (CPL), providing insight into the relationship between structural chirality and optical activity.

1 | Introduction

Supramolecular polymers, formed through the reversible, noncovalent interaction of monomeric units, represent a dynamic and versatile class of materials [1–3]. These polymers exhibit unique properties such as tunable optical activity, mechanical robustness, and environmental responsiveness, making them highly attractive for applications in material science, nanotechnology, and biomedical fields [3–6]. A critical aspect of supramolecular polymer design is the control of helicity—the handedness of the helical structures that these polymers can adopt [7–9]. Helicity control is not only fundamental to understanding the assembly process but also crucial for dictating the macroscopic properties of the material, such as its optical activity, particularly in the context of circular dichroism (CD) and circularly polarized luminescence (CPL). The ability to precisely control helicity in supramolecular polymers allows for the design of materials with specific chiroptical properties, which are essential for applications in enantioselective sensing, chiral photonics, and optoelectronic devices [10, 11].

Controlling the polymerization pathway is crucial for tailoring the structural and functional properties of the supramolecular materials. For instance, S. J. George and coworkers showed that in supramolecular polymerization based on chiral monomers, metastable assemblies grow into thermodynamically stable fiber

This is an open access article under the terms of the Creative Commons Attribution License, which permits use, distribution and reproduction in any medium, provided the original work is properly cited.

© 2025 The Author(s). *Aggregate* published by SCUT, AIEI, and John Wiley & Sons Australia, Ltd.

structures over time, and implemented fiber lengths that can be controlled by the ratio of seed concentration to monomer concentration through seeded living supramolecular polymerization [12]. Afterward, in 2024, a study on the precise synthesis of supramolecular polymers with CPL functionality in aqueous solutions was reported, and they implemented fixed CPL properties through length control and chiral information transfer [13]. Porphyrins, well known for their rich photophysical characteristics and structural versatility, have emerged as ideal building blocks for constructing complex supramolecular assemblies. Their ability to participate in diverse noncovalent interactions enables the formation of elaborate supramolecular polymers, making them excellent platforms for investigating pathway complexity in supramolecular polymerization processes [14–18]. The interplay between different noncovalent forces can lead to multiple assembly pathways and kinetic traps. Understanding and exploiting these pathways is critical to precisely controlling the structure and function of supramolecular polymers.

This study investigates the supramolecular polymerization of porphyrin dyads (PDs; Figure 1a), focusing on the pathway complexity involved in their assembly process. Due to this pathway complexity, PDs can form both kinetically metastable nanoparticles ($\mathbf{PD_{Particle}}$) and thermodynamically stable helical fibers ($\mathbf{PD_{Fiber}}$). The optical properties, specifically absorption and emission, of these two distinct supramolecular structures were systematically investigated. By tuning kinetic parameters and environmental conditions, we aim to control helicity of the resulting fibrous assemblies, thereby advancing our understanding of structure–property relationships in dynamic supramolecular systems. Notably, this work differs from previous studies by directly correlating the assembly pathway with ON/OFF control of the CPL, achieved through the use of chiral auxiliaries and temperature control. In this way, the study introduces a new dimension of functional control, namely, the modulation of optical activity based on the supramolecular assembly pathway.

The insights gained from this research contribute to the broader field of supramolecular chemistry, offering strategies for the rational design of functional materials with programmable and responsive properties.

2 | Results and Discussion

2.1 | Molecular Designs of PDs and Helical Fibrous Assembly Formation

Zinc porphyrin–based PDs were specifically designed as monomeric building blocks for supramolecular polymers [19]. Alkyl chains were introduced to the zinc porphyrin units to enhance the solubility of the PDs. The two planar zinc porphyrin units are connected via a rigid diacetylene bridge, which maintains a consistent spacing between the porphyrin units. In addition, two amide bonds link the porphyrin units to the diacetylene bridge, facilitating hydrogen-bonding interactions that drive the formation of fibrous assemblies.

Upon heating the **PD** in methylcyclohexane (MCH) to 373 K, a sharp Soret band absorption with a maximum wavelength (λ_{max}) at 417 nm was observed, indicating the disassembly of the **PD** into its monomeric form ($\mathbf{PD_{Mono}}$) (Figure 1b). When the solution was gradually cooled to 293 K at a rate of 1.0 K/min, the sharp Soret absorption band of **PD** gradually broadened and split into two distinct bands (λ_{max} = 409 and 429 nm). Transmission electron microscopy (TEM) and atomic force microscopy (AFM) revealed the formation of fibrous supramolecular polymers ($\mathbf{PD_{Fiber}}$) (Figure 1c). According to exciton coupling described by Kasha's principle [20, 21], the splitting of Soret band is attributed to exciton coupling between two orthogonally oriented transition dipoles of the porphyrin units within $\mathbf{PD_{Fiber}}$. During the formation of $\mathbf{PD_{Fiber}}$, the porphyrin building blocks adopt a twisted stacking, leading to the formation of helical supramolecular polymers (Figure 1d). The diacetylene bridge ensures sufficient spacing between the porphyrin units, enabling the clear observation of helical handedness in AFM images. Because **PD** is inherently achiral, the AFM images exhibit a random distribution of both *M* and *P* helices with a regular pitch of approximately 32 nm [19].

2.2 | Pathway Complexity of Supramolecular Polymerization

The absorption of **PD** was monitored upon cooling and successive heating between 373 and 293 K. Upon subsequent heating at the same rate of 1.0 K/min, the absorption spectrum of $\mathbf{PD_{Fiber}}$ gradually reverted to that of $\mathbf{PD_{Mono}}$. The spectral changes observed during the transition from $\mathbf{PD_{Mono}}$ to $\mathbf{PD_{Fiber}}$ and back exhibited thermal hysteresis, suggesting that the supramolecular polymerization and depolymerization pathways are not identical. To quantify these changes, the temperature-dependent degree of aggregation was estimated by monitoring the apparent absorption at 418.0 nm under different cooling and heating rates (Figure S1). When the cooling rate was increased to 10.0 K/min, more pronounced thermal hysteresis was observed compared to the slower cooling rate. In contrast, the heating curves remained consistent in shape regardless of the heating rate, indicating that the depolymerization pathway is relatively insensitive to the rate of temperature change.

Given the increased thermal hysteresis with faster cooling rates, a rapid cooling experiment was conducted by immersing a hot solution of $\mathbf{PD_{Mono}}$ in ice-cold water directly and resting for 5 min to fully cool down. The fast-cooled product displayed a distinct feature: a redshifted Soret band absorption with λ_{max} at 430 nm (Figure 2a). Furthermore, AFM and scanning electron microscopy (SEM) imaging of the fast-cooled product, spin-coated onto a mica substrate, revealed the formation of spherical nanoparticles ($\mathbf{PD_{Particle}}$) (Figure 2b). These observations demonstrate that the cooling rate significantly affects the supramolecular polymerization pathways, with slow cooling favoring the formation of $\mathbf{PD_{Fiber}}$ and rapid cooling leading to the formation of $\mathbf{PD_{Particle}}$, thereby explaining the pathway complexity inherent in the supramolecular polymerization of **PD** as depicted in Figure 2c [15].

2.3 | Transformation From $\mathbf{PD_{Particle}}$ to $\mathbf{PD_{Fiber}}$

The absorption spectrum of $\mathbf{PD_{Particle}}$ (2.0 μM in MCH), obtained through rapid cooling, was monitored at 293 K to investigate its

26924560, 2025, 8, Downloaded from https://onlinelibrary.wiley.com/doi/10.1002/agt2.70090 by Ewha Womans University Library, Wiley Online Library on [02/12/2025]. See the Terms and Conditions (https://onlinelibrary.wiley.com/terms-and-conditions) on Wiley Online Library for rules of use; OA articles are governed by the applicable Creative Commons License

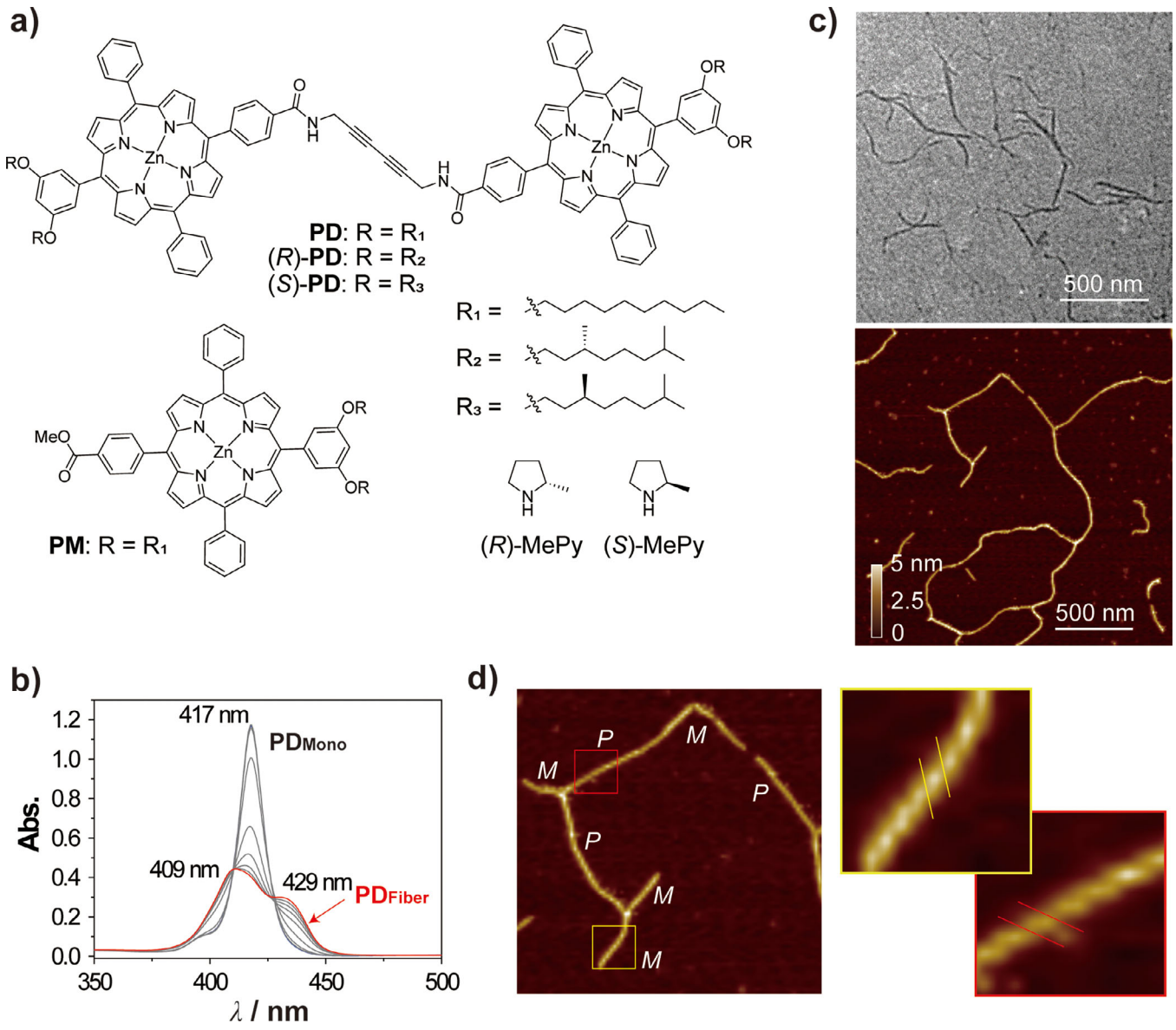


FIGURE 1 | Molecular structures and fibrous supramolecular polymer formation. (a) Molecular structures used in this study, (b) absorption spectral changes of **PD** (2.0 μM in MCH) upon cooling from 373 to 293 K at a rate of 1.0 K/min, (c) TEM and AFM images of supramolecular polymers, and (d) AFM images for typical *M* and *P* helices.

stability. Over time, the absorption spectrum gradually shifted, matching that of $\mathbf{PD}_{\mathbf{Fiber}}$, indicating that $\mathbf{PD}_{\mathbf{Particle}}$ is a metastable state (Figure 3a). Morphological analysis using AFM further confirmed this transformation, revealing the gradual conversion of spherical particles into helical fibers (Figure 3b). This suggests that $\mathbf{PD}_{\mathbf{Particle}}$, formed via fast cooling, is a kinetic product that gradually transitions into the more thermodynamically stable $\mathbf{PD}_{\mathbf{Fiber}}$. To further explore this transformation, concentration-dependent studies were conducted at 293 K (Figure S2). Interestingly, the transformation rate was independent of concentration, implying that the transformation from $\mathbf{PD}_{\mathbf{Particle}}$ to $\mathbf{PD}_{\mathbf{Fiber}}$ is an off-pathway process. This suggests that $\mathbf{PD}_{\mathbf{Particle}}$ does not directly convert into $\mathbf{PD}_{\mathbf{Fiber}}$. Instead, $\mathbf{PD}_{\mathbf{Particle}}$ first dissociates into $\mathbf{PD}_{\mathbf{Mono}}$, which then undergoes supramolecular polymerization to form $\mathbf{PD}_{\mathbf{Fiber}}$, as depicted in Figure 3c. Temperature-dependent studies using a 2.0 μM solution of **PD** were also conducted to examine the effect of temperature on the transformation rate (Figure 3d). In this experiment, $\mathbf{PD}_{\mathbf{Particle}}$ was first prepared by fast cooling and then immediately transferred to a temperature controller-equipped UV-Vis spectrometer, where the time-dependent changes in the absorption spectrum were monitored at a controlled temperature. The absorbance at 309.5 nm was specifically tracked to quantify the formation rate of $\mathbf{PD}_{\mathbf{Fiber}}$, as this wavelength corresponds to the characteristic absorption of the fibrous state. The results showed that the transformation rate from $\mathbf{PD}_{\mathbf{Particle}}$ to $\mathbf{PD}_{\mathbf{Fiber}}$ accelerated with increasing temperature.

The thermodynamic parameters for the supramolecular polymerization of $\mathbf{PD}_{\mathbf{Mono}}$ into $\mathbf{PD}_{\mathbf{Fiber}}$ were previously estimated from temperature-dependent aggregation curves, yielding values of $\Delta H = -87.1$ kJ/mol and $\Delta S = -134$ J/mol·K [19]. Since $\mathbf{PD}_{\mathbf{Particle}}$ is a kinetic metastable product, the ΔH for its formation is expected to be less exothermic than −87.1 kJ/mol. However,

26924560, 2025, 8, Downloaded from https://onlinelibrary.wiley.com/doi/10.1002/agt2.70090 by Ewha Womans University Library, Wiley Online Library on [02/12/2025]. See the Terms and Conditions (https://onlinelibrary.wiley.com/terms-and-conditions) on Wiley Online Library for rules of use; OA articles are governed by the applicable Creative Commons License

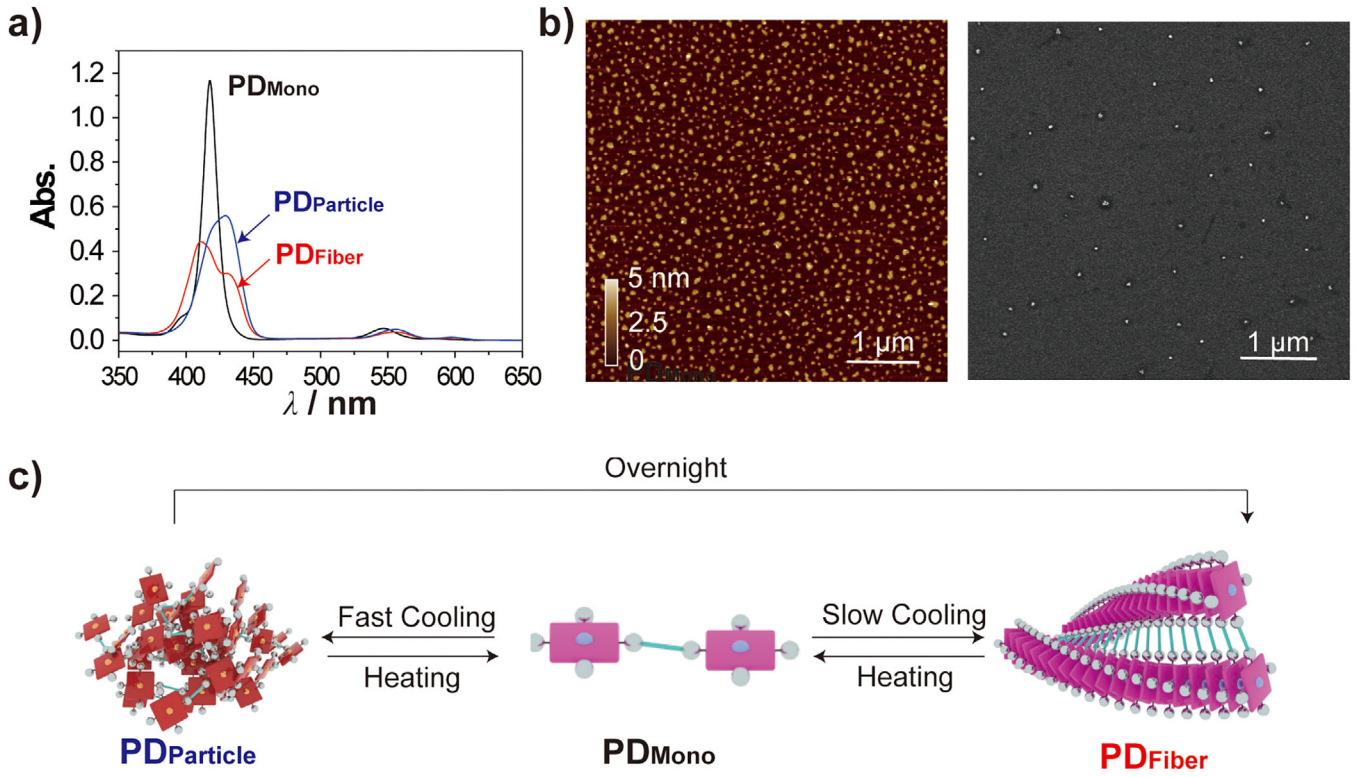


FIGURE 2 | Pathway complexity of **PD**. (a) Absorption spectra of $\mathbf{PD}_{\mathbf{Mono}}$, $\mathbf{PD}_{\mathbf{Particle}}$, and $\mathbf{PD}_{\mathbf{Fiber}}$, (b) AFM and SEM images of $\mathbf{PD}_{\mathbf{Particle}}$, and (c) schematic expression of pathway complexity.

due to its metastable nature, a precise estimation of ΔH and ΔS for $\mathbf{PD}_{\mathbf{Particle}}$ formation was not possible. Given that the transformation from $\mathbf{PD}_{\mathbf{Particle}}$ to $\mathbf{PD}_{\mathbf{Fiber}}$ involves an off-pathway process, this transformation can be understood as a two-step mechanism: (1) dissociation of $\mathbf{PD}_{\mathbf{Particle}}$ into $\mathbf{PD}_{\mathbf{Mono}}$ and (2) supramolecular polymerization of $\mathbf{PD}_{\mathbf{Mono}}$ into $\mathbf{PD}_{\mathbf{Fiber}}$. The first step is endothermic and is likely the rate-determining step in the overall transformation process. If the polymerization step (second step) is much faster than the dissociation step, the transformation kinetics can be approximated as a first-order reaction. Using this assumption, the rate constants for the transformation from $\mathbf{PD}_{\mathbf{Particle}}$ to $\mathbf{PD}_{\mathbf{Fiber}}$ were estimated from temperature-dependent transformation curves through nonlinear curve fitting of first-order kinetics. The activation energy (E_{act}) for the dissociation step was then calculated using the Arrhenius equation, yielding a value of 116.7 kJ/mol. This E_{act} is slightly higher than the ΔH for $\mathbf{PD}_{\mathbf{Fiber}}$ formation, highlighting the energetic barrier associated with the dissociation process.

2.4 | Helicity Control of Supramolecular Polymers

As previously discussed, achiral **PD** exhibited a random distribution of both *M* and *P* helices, as observed on AFM images. This result was supported by the results of CD measurement, which show a CD-silent spectrum, indicating the absence of chirality (Figure S3). To achieve controlled helicity in supramolecular polymers, chiral alkyl chains were introduced into the PDs, producing two distinct variants: (*S*)-**PD** and (*R*)-**PD** (Figure 1a), corresponding to the enantiomers of the chiral alkyl groups employed. Upon slow cooling of the solution of these chiral PDs from 373 to 293 K, the formation of fibrous supramolecular polymers ($\mathbf{PD}_{\mathbf{Fiber}}$) was observed. Likewise, fast cooling of the chiral **PD**s resulted in the formation of $\mathbf{PD}_{\mathbf{Particle}}$s. The absorption changes during fast and slow cooling processes of (*S*)-**PD** and (*R*)-**PD** were identical to that of achiral **PD**, indicating that both (*S*)-**PD** and (*R*)-**PD** exhibit the same pathway complexity as achiral **PD** (Figure S4).

Despite the thermal behavior of chiral PDs being identical to that of achiral **PD**, the introduction of chiral alkyl groups effectively induced the preferential formation of a specific helical sense. Specifically, (*S*)-$\mathbf{PD}_{\mathbf{Fiber}}$ favored the formation of *M* helices, while (*R*)-$\mathbf{PD}_{\mathbf{Fiber}}$ favored the formation of *P* helices. AFM images of (*S*)-$\mathbf{PD}_{\mathbf{Fiber}}$ and (*R*)-$\mathbf{PD}_{\mathbf{Fiber}}$ demonstrate the preferences of *M* and *P* helices, respectively (Figure 4a). Based on the helical handedness observed in AFM images, (*S*)-$\mathbf{PD}_{\mathbf{Fiber}}$ exhibited an enantiomeric excess (ee) of 45% for *P* helix, while (*R*)-$\mathbf{PD}_{\mathbf{Fiber}}$ showed an ee of 40% for *M* helix. These results indicate that the introduction of chiral side chains induces a clear chiral bias in the supramolecular polymerization process. CD spectra of $\mathbf{PD}_{\mathbf{Fiber}}$s formed by (*S*)-**PD** and (*R*)-**PD** also exhibited strong Cotton effects with opposite signs, confirming the formation of chiral assemblies (Figure 4b). In contrast, the solutions of (*S*)-**PD** in tetrahydrofuran (THF) showed no CD signal, indicating the CD signals originated from supramolecular assembly formation (Figure S5). These results indicate that the stereo genic centers of the chiral alkyl chains direct the twisted helical stacking of porphyrin units along the diacetylene bridges, resulting in supramolecular structures with defined helices. On the other hand, (*S*)-$\mathbf{PD}_{\mathbf{Particle}}$s formed by fast cooling did not show CD

26924560, 2025, 8, Downloaded from https://onlinelibrary.wiley.com/doi/10.1002/agt2.70090 by Ewha Womans University Library, Wiley Online Library on [02/12/2025]. See the Terms and Conditions (https://onlinelibrary.wiley.com/terms-and-conditions) on Wiley Online Library for rules of use; OA articles are governed by the applicable Creative Commons License

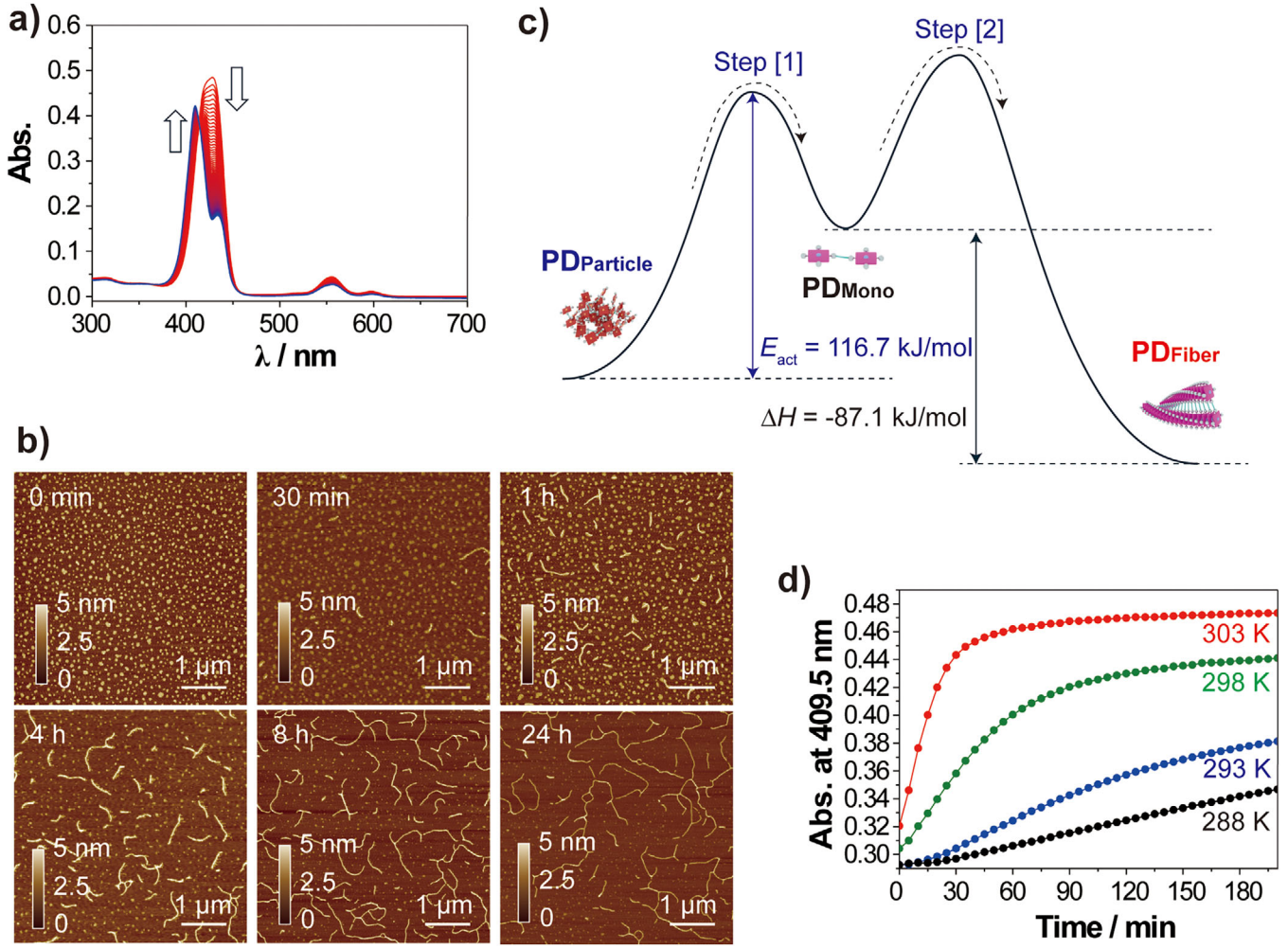


FIGURE 3 | Transformation from $\mathbf{PD_{Particle}}$ to $\mathbf{PD_{Fiber}}$. (a) Absorption spectral change from $\mathbf{PD_{Particle}}$ to $\mathbf{PD_{Fiber}}$ at 293 K for 24 h with 30 min intervals, (b) AFM images of morphological transformation from $\mathbf{PD_{Particle}}$ to $\mathbf{PD_{Fiber}}$. The solution of $\mathbf{PD_{Particle}}$ (2.0 μM in MCH) was stored at 293 K without any disturbance. (c) Pathway diagram of transformation from $\mathbf{PD_{Particle}}$ to $\mathbf{PD_{Fiber}}$, and (d) Absorption change at 409.5 nm under various temperatures.

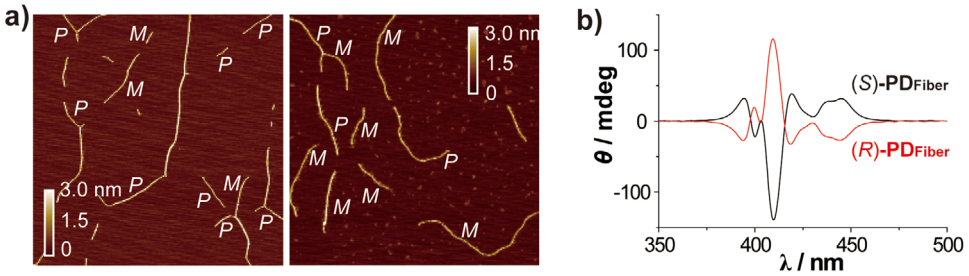


FIGURE 4 | Helicity control of **PD**s by the introduction of chiral alkyl chains. (a) AFM images of PD_{Fiber}s obtained from (*S*)-**PD** (left) and (*R*)-**PD** (right), and (b) CD spectra of (*S*)-$\mathbf{PD_{Fiber}}$ and (*R*)-$\mathbf{PD_{Fiber}}$.

signals, indicating the chiral alkyl chains did not influence the ordering of porphyrin units in $\mathbf{PD_{Particle}}$s (Figure S5).

Zinc porphyrins are known for their ability to coordinate with various ligands through axial coordination, which can significantly influence their physicochemical properties [22–25]. The coordination of ligands to the central zinc ion can alter the steric environment of the porphyrin, thereby affecting supramolecular polymerization [26, 27]. If these ligands bind tightly to the porphyrin building blocks, they may inhibit the formation of $\mathbf{PD_{Fiber}}$. To investigate this, the supramolecular polymerization of **PD** was explored in the presence of 2-methyl pyrrolidine (MePy; Figure 1a). To estimate the binding constant of this axial coordination, MePy was spectroscopically titrated with monomeric porphyrin **PM** (Figure 1a), a structural fragment of **PD**. The absorption spectrum of PM showed a

26924560, 2025, 8, Downloaded from https://onlinelibrary.wiley.com/doi/10.1002/agt2.70090 by Ewha Womans University Library, Wiley Online Library on [02/12/2025]. See the Terms and Conditions (https://onlinelibrary.wiley.com/terms-and-conditions) on Wiley Online Library for rules of use; OA articles are governed by the applicable Creative Commons License

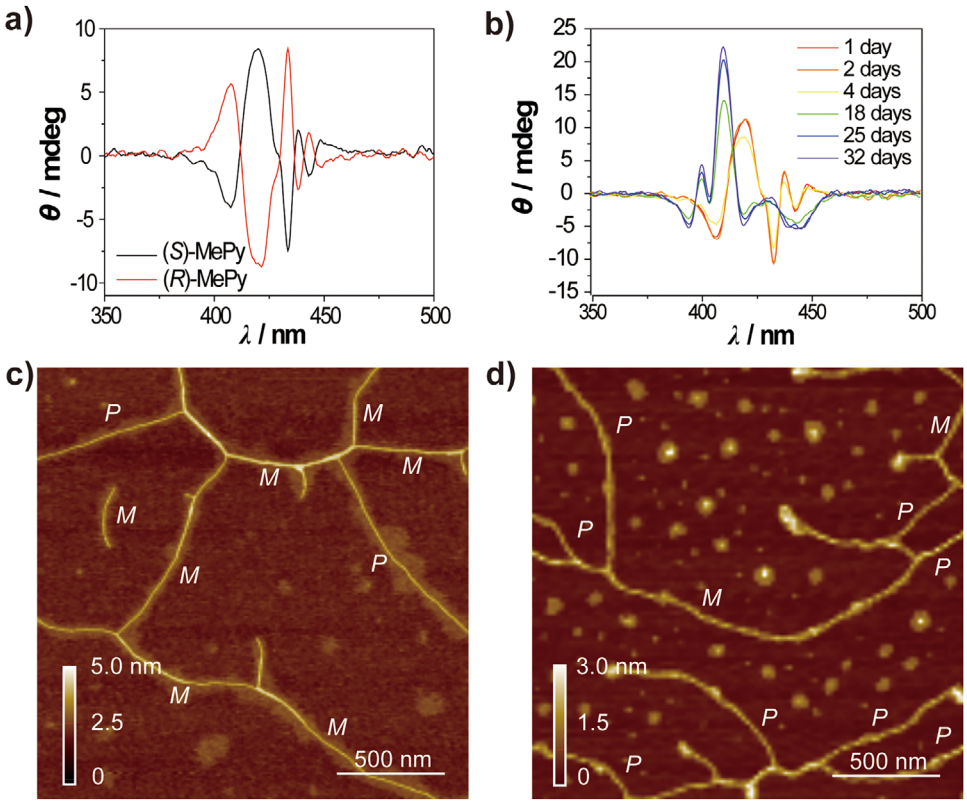


FIGURE 5 | Helicity control of $\mathbf{PD_{Fiber}}$s by axial coordination of chiral ligands. (a) Induced CD signals of PDs by axial coordination of chiral MePy, and (b) CD spectral change of **PD** from (*S*)-MePy-coordinated **PD** to *P* helicity-enriched $\mathbf{PD_{Fiber}}$. AFM image of $\mathbf{PD_{Fiber}}$ formed in the presence of (c) (*S*)-MePy and (d) (*R*)-MePy.

red shift by the addition of MePy with isosbestic points at 424.0, 555.0, and 587.5 nm (Figure S6). The binding constant was determined to be 2.5×10^5 M^{-1} at 20°C through non-linear curve fitting using commercial Hypspec software, with a calculated ΔG of −29.3 kJ/mol. The ΔG for MePy binding to zinc porphyrin was smaller than that of supramolecular polymerization.

To further assess the impact of MePy, 10 equivalents of MePy were added to a 2.0 μM **PD** solution. This solution was then slowly cooled down from 373 to 293 K at a rate of 1.0 K/min. The **PD** solution exhibited redshifted absorption, indicating the binding of MePy to the zinc porphyrin units in **PD**. The axial coordination of MePy to **PD** suppressed the growth of $\mathbf{PD_{Fiber}}$. It is noteworthy that the binding of MePy to the zinc porphyrin was characterized by a ΔG of −29.3 kJ/mol, which is greatly less negative than the ΔG for the supramolecular polymerization process, as inferred from the thermodynamic parameters of $\Delta H = -87.1$ kJ/mol and $\Delta S = -134$ J/mol·K. Therefore, the equilibrium should eventually shift toward $\mathbf{PD_{Fiber}}$ formation. As expected, the **PD** solution containing 10 equivalents of MePy gradually formed $\mathbf{PD_{Fiber}}$, although it required a much longer time. As shown in Figure 5a, the CD signals of **PD** initially show different shapes with $\mathbf{PD_{Fiber}}$, which is caused by the axial coordination of chiral MePy to porphyrin building blocks. The initial CD signal of **PD** was gradually changed to the shape of $\mathbf{PD_{Fiber}}$, indicating the generation of thermodynamically stable $\mathbf{PD_{Fiber}}$ (Figure 5b). This slow, gradual formation suggests that a kinetic barrier to polymerization is present but is eventually overcome as the system reaches thermodynamic equilibrium.

In addition, because MePy is a chiral compound, its presence during the slow transformation into $\mathbf{PD_{Fiber}}$ influences the helicity of the resulting supramolecular polymer. Specifically, **PD** favored the formation of *M* helices in the presence of (*R*)-MePy, whereas the formation of *P* helices was favored in the presence of (*S*)-MePy. The chirality of MePy induces a preference for the formation of one helical sense over the other. This observation was confirmed by CD spectroscopy, where the initial **PD** solution containing both (*R*)-MePy and (*S*)-MePy exhibited induced CD signals due to the axial coordination of chiral ligands with opposite signs (Figure 5a). Over time, the CD signals were gradually shifted toward those characteristic of *M* helices or *P* helices, depending on the chirality of MePy (Figure 5b). These results highlight MePy's dual role as both a kinetic inhibitor and a chiral inducer that directs the helicity of the resulting supramolecular polymer. AFM observation further supported these findings, revealing distinct helical structures for $\mathbf{PD_{Fiber}}$s formed in the presence of (*R*)-MePy and (*S*)-MePy. The AFM images showed clear *M* helices in the samples with (*R*)-MePy and *P* helices with (*S*)-MePy, with the helical pitch remaining consistent with those observed in the achiral **PD** system (Figure 5c,d). The combination of CD and AFM data indicates the precise control over helicity that can be achieved through the introduction of chiral MePy, confirming that the supramolecular polymerization process can be finely tuned to produce enantioselective assemblies.

26924560, 2025, 8, Downloaded from https://onlinelibrary.wiley.com/doi/10.1002/agt2.70090 by Ewha Womans University Library, Wiley Online Library on [02/12/2025]. See the Terms and Conditions (https://onlinelibrary.wiley.com/terms-and-conditions) on Wiley Online Library for rules of use; OA articles are governed by the applicable Creative Commons License

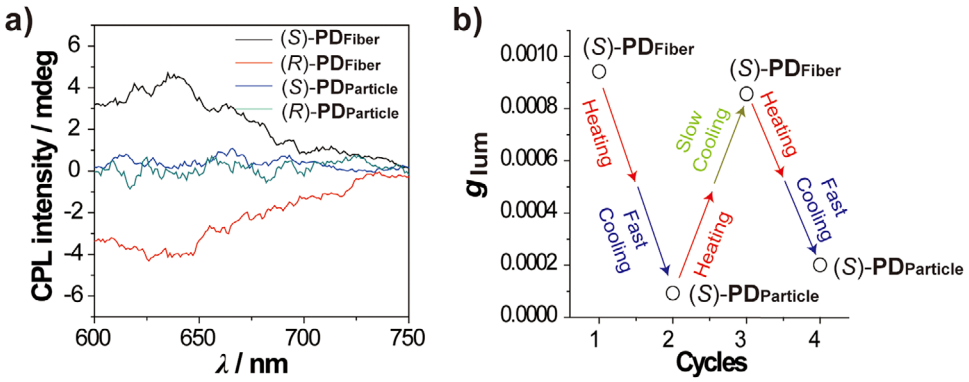


FIGURE 6 | Kinetic control of CPL emission. (a) CPL emission of $\mathbf{PD_{Fiber}}$s and $\mathbf{PD_{Particle}}$s (b) CPL control by fast and slow cooling.

2.5 | Circularly Polarized Luminescence of Helical $\mathbf{PD_{Fiber}}$s

After successful control of the handedness of the helical supramolecular polymer formed from chiral **PD**, we observed strong fluorescence from the resulting helices (Figure S7). Based on these results, we presumed that chiral $\mathbf{PD_{Fiber}}$s may emit CPL. To investigate this, we measured the CPL emission of both $\mathbf{PD_{Fiber}}$s and $\mathbf{PD_{Particle}}$s. The $\mathbf{PD_{Fiber}}$s derived from (*S*)-**PD** and (*R*)-**PD** exhibited opposite CPL signals, reflecting their enantioselective helical structures. The anisotropy factor of CPL, g_{lum}, quantifies the degree of chiral dissymmetry in emission, calculated using the equation:

$$g_{lum} = \frac{2(I_L - I_R)}{I_L + I_R}$$

where I_L and I_R are the intensities of left- and right-handed circularly polarized emissions, respectively [28, 29]. The g_{lum} value for the $\mathbf{PD_{Fiber}}$s was estimated to be 1.2×10^3, comparable to other supramolecular assemblies reported in the literature [30–34]. In contrast, $\mathbf{PD_{Particle}}$s obtained from (*S*)-**PD** and (*R*)-**PD** did not exhibit CPL, indicating that the porphyrin units within the $\mathbf{PD_{Particle}}$s are randomly oriented without a chiral arrangement. On AFM images from Figure 4a, (*S*)-$\mathbf{PD_{Fiber}}$ and (*R*)-$\mathbf{PD_{Fiber}}$ showed 45% and 40% ee values, respectively. Although these values do not represent complete helicity bias, they indicate a preference for one helical sense, which is consistent with the observed CD signals. This helicity bias, combined with the strong fluorescence of porphyrin moieties, supports the emergence of CPL activity. The estimated g_{lum} value is modest but comparable to those reported for other supramolecular CPL systems. Because the stereogenic center is located on the peripheral alkyl chains, far from the porphyrin building blocks, it has a limited effect on the chiral arrangement of the porphyrin fluorophores. We anticipate that future studies, introducing the stereogenic center closer to the porphyrin core, could enhance both helicity bias and CPC efficiency.

Given the pathway complexity of PDs, CPL emission can be kinetically regulated by manipulating the cooling rate of the solution (Figure 6a). Specifically, repeated cycles of fast and slow cooling resulted in the reversible control of CPL emission, allowing it to be switched ON and OFF multiple times (Figure 6b).

In addition, the helicity of $\mathbf{PD_{Fiber}}$s formed from achiral **PD** was controlled by the presence of chiral MePy, leading to distinct CPL signals. CPL measurements conducted after the slow transformation of a **PD** solution containing MePy into $\mathbf{PD_{Fiber}}$s revealed that the $\mathbf{PD_{Fiber}}$s exhibited CPL consistent with the helicity induced by the chiral auxiliary. Specifically, the $\mathbf{PD_{Fiber}}$ formed in the presence of (*R*)-MePy emitted CPL with a negative sign corresponding to *M* helices, as observed via AFM and CD spectroscopy. In contrast, $\mathbf{PD_{Fiber}}$s formed in the presence of (*S*)-MePy showed a positive CPL signal, aligning with the formation of *P* helices (Figure S8). This correlation between CPL signals and the helicity of the $\mathbf{PD_{Fiber}}$s indicates that the chiral supramolecular polymerization process directly influences the material's luminescence properties. The CPL activity highlights the significant role of the chiral environment provided by MePy, which not only dictates the structural chirality of the fibers but also imparts optical activity at the macroscopic level.

3 | Conclusion

This study on the supramolecular polymerization of zinc **PD**s features the profound influence of molecular design and environmental conditions on the assembly and optical properties of the resulting structures. The ability to control the helicity of $\mathbf{PD_{Fiber}}$s through the introduction of chiral alkyl chains and external ligands like MePy demonstrates the versatility of supramolecular systems in producing enantioselective assemblies with distinct optical activities. Our findings highlight the complexity of supramolecular polymerization pathways, where the rate of cooling and the presence of chiral auxiliaries dictate the formation of either helical fibers or spherical particles. The transformation from kinetically trapped $\mathbf{PD_{Particle}}$s to thermodynamically stable $\mathbf{PD_{Fiber}}$s further elucidates the energy landscape governing these processes, offering a deeper understanding of the factors that drive and inhibit supramolecular assembly. Moreover, the observation of CPL in helical $\mathbf{PD_{Fiber}}$s emphasizes the potential of these materials for applications in chiroptical devices. The ability to reversibly switch CPL emissions ON and OFF by controlling the polymerization kinetics opens new avenues for the development of smart materials with tunable optical properties. The correlation between the helicity of supramolecular polymers and their CPL emission underscores the significance of chirality in designing functional supramolecular systems.

26924560, 2025, 8, Downloaded from https://onlinelibrary.wiley.com/doi/10.1002/agt2.70090 by Ewha Womans University Library, Wiley Online Library on [02/12/2025]. See the Terms and Conditions (https://onlinelibrary.wiley.com/terms-and-conditions) on Wiley Online Library for rules of use; OA articles are governed by the applicable Creative Commons License

The ability to achieve and control CPL in these supramolecular systems has significant implications for the development of advanced chiroptical materials. Such materials are of great interest in fields ranging from optoelectronics to bioimaging, where the control of light polarization is crucial. The results presented here demonstrate that by carefully selecting chiral auxiliaries like MePy, it is possible to fine-tune both the structural and optical properties of supramolecular polymers, paving the way for new applications in these emerging technologies.

Acknowledgments

This work was supported by the National Research Foundation (NRF) grant (RS-2025-00514482, RS-2024-00345550) funded by the Ministry of Science and ICT (MSIT), Korea.

Conflicts of Interest

The authors declare no conflicts of interest.

References

1. L. Brunsveld, B. J. Folmer, E. W. Meijer, and R. P. Sijbesma, "Supramolecular Polymers," *Chemical Reviews* 101 (2001): 4071–4098.

2. B. Qin, Z. Yin, X. Tang, et al., "Supramolecular Polymer Chemistry: From Structural Control to Functional Assembly," *Progress in Polymer Science* 100 (2020): 101167.

3. L. Yang, X. Tan, Z. Wang, and X. Zhang, "Supramolecular Polymers: Historical Development, Preparation, Characterization, and Functions," *Chemical Reviews* 115 (2015): 7196–7239.

4. T. Aida, E. Meijer, and S. Stupp, "Functional Supramolecular Polymers," *Science* 335 (2012): 813–817.

5. R. Dong, Y. Zhou, X. Huang, X. Zhu, Y. Lu, and J. Shen, "Functional Supramolecular Polymers for Biomedical Applications," *Advanced Materials* 27 (2015): 498–526.

6. H. Wang, X. Ji, Z. Li, and F. Huang, "Fluorescent Supramolecular Polymeric Materials," *Advanced Materials* 29 (2017): 1606117.

7. M. M. Smulders, A. P. Schenning, and E. Meijer, "Insight Into the Mechanisms of Cooperative Self-Assembly: The "Sergeants-and-Soldiers" Principle of Chiral and Achiral C3-Symmetrical Discotic Triamides," *Journal of the American Chemical Society* 130 (2008): 606–611.

8. J. van Gestel, A. R. Palmans, B. Titulaer, J. A. Vekemans, and E. Meijer, "Majority-Rules″ Operative in Chiral Columnar Stacks of C_3-Symmetrical Molecules" *Journal of the American Chemical Society* 127 (2005): 5490–5494.

9. P. Xing and Y. Zhao, "Controlling Supramolecular Chirality in Multicomponent Self-Assembled Systems," *Accounts of Chemical Research* 51 (2018): 2324–2334.

10. A. Das, S. Ghosh, and S. J. George, "Chiroptical Amplification of Induced Circularly Polarized Luminescence in Nucleotide-Templated Supramolecular Polymer," *Angewandte Chemie* 135 (2023): e202308281.

11. L. López-Gandul, C. Naranjo, C. Sánchez, et al., "Stereomutation and Chiroptical Bias in the Kinetically Controlled Supramolecular Polymerization of Cyano-Luminogens," *Chemical Science* 13 (2022): 11577–11584.

12. S. Sarkar, A. Sarkar, and S. J. George, "Stereoselective Seed-Induced Living Supramolecular Polymerization," *Angewandte Chemie International Edition* 59 (2020): 19841–19845.

13. S. Patra, S. Dhiman, and S. J. George, "Precision Synthesis of Circularly Polarized Luminescence Active Organic Assemblies in Aqueous Media via Efficient Living Supramolecular Polymerization," *Chemistry of Materials* 36 (2024): 9460–9468.

14. T. Fukui, S. Kawai, S. Fujinuma, et al., "Control Over Differentiation of a Metastable Supramolecular Assembly in One and Two Dimensions," *Nature Chemistry* 9 (2017): 493–499.

15. P. A. Korevaar, S. J. George, A. J. Markvoort, et al., "Pathway Complexity in Supramolecular Polymerization," *Nature* 481 (2012): 492–496.

16. S. Ogi, V. Stepanenko, J. Thein, and F. Würthner, "Impact of Alkyl Spacer Length on Aggregation Pathways in Kinetically Controlled Supramolecular Polymerization," *Journal of the American Chemical Society* 138 (2016): 670–678.

17. M. Wehner, M. I. S. Röhr, V. Stepanenko, and F. Würthner, "Control of Self-Assembly Pathways Toward Conglomerate and Racemic Supramolecular Polymers," *Nature Communications* 11 (2020): 5460.

18. M. Wehner and F. Würthner, "Supramolecular Polymerization Through Kinetic Pathway Control and Living Chain Growth," *Nature Reviews Chemistry* 4 (2020): 38–53.

19. H. Lee, M. Lee, J. H. Hwang, I. Kim, E. Lee, and W.-D. Jang, "Recognition of Atomic-Level Difference in Porphyrin Dyads for Self-Sorted Supramolecular Polymer Growth," *Nanoscale* 15 (2023): 18224–18232.

20. C. A. Hunter, J. K. Sanders, and A. J. Stone, "Exciton Coupling in Porphyrin Dimers," *Chemical Physics* 133 (1989): 395–404.

21. L. T. Bergendahl and M. J. Paterson, "Excited States of Porphyrin and Porphycene Aggregates: Computational Insights," *Computational and Theoretical Chemistry* 1040 (2014): 274–286.

22. K. Kinjo, T. Hirao, S. I. Kihara, Y. Katsumoto, and T. Haino, "Supramolecular Porphyrin Copolymer Assembled Through Host–Guest Interactions and Metal–Ligand Coordination," *Angewandte Chemie* 127 (2015): 15043–15047.

23. T. Kojima, T. Nakanishi, T. Honda, R. Harada, M. Shiro, and S. Fukuzumi, "Impact of Distortion of Porphyrins on Axial Coordination in (Porphyrinato)Zinc(II) Complexes With Aminopyridines as Axial Ligands," *European Journal of Inorganic Chemistry* 2009 (2009): 727–734.

24. H. Lee, H. Park, D. Y. Ryu, and W.-D. Jang, "Porphyrin-Based Supramolecular Polymers," *Chemical Society Reviews* 52 (2023): 1947–1974.

25. C. O. Obondi, G. N. Lim, Y. Jang, et al., "Charge Stabilization in High-Potential Zinc Porphyrin-Fullerene via Axial Ligation of Tetrathiafulvalene," *Journal of Physical Chemistry C* 122 (2018): 13636–13647.

26. H. Lee, D. Lee, I. Kim, E. Lee, and W.-D. Jang, "Formation of Supramolecular Polymers From Porphyrin Tripods," *Macromolecules* 53 (2020): 8060–8067.

27. D. Yim, J. Sung, S. Kim, et al., "Guest-Induced Modulation of the Energy Transfer Process in Porphyrin-Based Artificial Light Harvesting Dendrimers," *Journal of the American Chemical Society* 139 (2017): 993–1002.

28. G. Longhi, E. Castiglioni, J. Koshoubu, G. Mazzeo, and S. Abbate, "Circularly Polarized Luminescence: A Review of Experimental and Theoretical Aspects," *Chirality* 28 (2016): 696–707.

29. Y. Sang, J. Han, T. Zhao, P. Duan, and M. Liu, "Circularly Polarized Luminescence in Nanoassemblies: Generation, Amplification, and Application," *Advanced Materials* 32 (2020): 1900110.

30. H. Isla, M. Srebro-Hooper, M. Jean, et al., "Conformational Changes and Chiroptical Switching of Enantiopure Bis-Helicenic Terpyridine Upon Zn 2+ Binding," *Chemical Communications* 52 (2016): 5932–5935.

31. S. Ito, K. Ikeda, S. Nakanishi, Y. Imai, and M. Asami, "Concentration-Dependent Circularly Polarized Luminescence (CPL) of Chiral N,N′-Dipyrenyldiamines: Sign-Inverted CPL Switching Between Monomer and Excimer Regions Under Retention of the Monomer Emission for Photoluminescence," *Chemical Communications* 53 (2017): 6323–6326.

32. K. Nakabayashi, T. Amako, N. Tajima, M. Fujiki, and Y. Imai, "Non-classical Dual Control of Circularly Polarized Luminescence Modes of Binaphthyl–Pyrene Organic Fluorophores in Fluidic and Glassy Media," *Chemical Communications* 50 (2014): 13228–13230.

26924560, 2025, 8, Downloaded from https://onlinelibrary.wiley.com/doi/10.1002/agt2.70090 by Ewha Womans University Library, Wiley Online Library on [02/12/2025]. See the Terms and Conditions (https://onlinelibrary.wiley.com/terms-and-conditions) on Wiley Online Library for rules of use; OA articles are governed by the applicable Creative Commons License

33. N. Saleh, B. Moore, M. Srebro, et al., "Acid/Base-Triggered Switching of Circularly Polarized Luminescence and Electronic Circular Dichroism in Organic and Organometallic Helicenes," *Chemistry: A European Journal* 21 (2015): 1673–1681.

34. K. Takaishi, M. Yasui, and T. Ema, "Binaphthyl–Bipyridyl Cyclic Dyads as a Chiroptical Switch," *Journal of the American Chemical Society* 140 (2018): 5334–5338.

Supporting Information

Additional supporting information can be found online in the Supporting Information section.

Supporting file: agt270090-sup-0001-SupMat.docx

26924560, 2025, 8, Downloaded from https://onlinelibrary.wiley.com/doi/10.1002/agt2.70090 by Ewha Womans University Library, Wiley Online Library on [02/12/2025]. See the Terms and Conditions (https://onlinelibrary.wiley.com/terms-and-conditions) on Wiley Online Library for rules of use; OA articles are governed by the applicable Creative Commons License